2722–2732 Nucleic Acids Research, 2018, Vol. 46, No. 6 Published online 22 February 2018
doi: 10.1093/nar/gky084

Characterization of clinically used oral antiseptics as quadruplex-binding ligands

David R. Calabrese[1], Katherine Zlotkowski[1], Stephanie Alden[1], William M. Hewitt[1], Colleen M. Connelly[1], Robert M. Wilson[1], Snehal Gaikwad[2], Lu Chen[3], Rajarshi Guha[3], Craig J. Thomas[3], Beverly A. Mock[2] and John S. Schneekloth, Jr.[1,*]

[1]Chemical Biology Laboratory, National Cancer Institute, Frederick, MD 21702-1201, USA, [2]Laboratory of Cancer Biology and Genetics, National Cancer Institute, Bethesda, MD 20892-4258, USA and [3]Division of Preclinical Innovation, National Center for Advancing Translational Sciences, National Institutes of Health, Bethesda, MD, USA

Received December 14, 2017; Revised January 10, 2018; Editorial Decision January 28, 2018; Accepted February 20, 2018

ABSTRACT

Approaches to characterize the nucleic acid-binding properties of drugs and druglike small molecules are crucial to understanding the behavior of these compounds in cellular systems. Here, we use a Small Molecule Microarray (SMM) profiling approach to identify the preferential interaction between chlorhexidine, a widely used oral antiseptic, and the G-quadruplex (G4) structure in the *KRAS* oncogene promoter. The interaction of chlorhexidine and related drugs to the *KRAS* G4 is evaluated using multiple biophysical methods, including thermal melt, fluorescence titration and surface plasmon resonance (SPR) assays. Chlorhexidine has a specific low micromolar binding interaction with the G4, while related drugs have weaker and/or less specific interactions. Through NMR experiments and docking studies, we propose a plausible binding mode driven by both aromatic stacking and groove binding interactions. Additionally, cancer cell lines harbouring oncogenic mutations in the *KRAS* gene exhibit increased sensitivity to chlorhexidine. Treatment of breast cancer cells with chlorhexidine decreases KRAS protein levels, while a *KRAS* gene transiently expressed by a promoter lacking a G4 is not affected. This work confirms that known ligands bind broadly to G4 structures, while other drugs and druglike compounds can have more selective interactions that may be biologically relevant.

INTRODUCTION

Small molecules that bind to nucleic acids are powerful chemical tools that can control gene expression and have substantial potential as chemotherapeutics (1–5). While most modern medicinal chemistry focuses on protein targets, an increased understanding of the structure and function of non-coding nucleic acids suggests that oligonucleotides may be suitable targets for small molecules as well. Attempts to target B-DNA, for example with pyrrole-imidazole polyamides (6,7), have resulted in compounds with remarkable selectivity but have yet to yield a clinically used drug. While it is unlikely that approved drugs will bind to B-DNA with selectivity, little is known about how such drugs interact with other comparatively rare alternatively folded nucleic acid structures. Interactions with these structures could have profound effects in a cellular context and could result in unanticipated pharmacological consequences.

One structure that has received considerable interest as a small molecule target is the G-quadruplex (G4). G4s are non-B DNA structures with globular folds that occur in guanine-rich sequences. G4s are characterized by stacks of Hoogsteen-bonded guanine tetrads stabilized by central potassium ions and flanked by loop regions (8). DNA G4s have been identified in genome-wide structural probing studies using a G4-specific antibody (9), as well as in a chemical probing approach employing ss-DNA seq (10), and are estimated to exist in several thousand locations in the human genome. Furthermore, G4s have been implicated in regulating gene expression (11). Folded DNA G4s are enriched in nucleosome-depleted regions of the genome, occurring primarily in the promoter regions of both oncogenes and developmental genes that are normally silent in differentiated cells (9). Although the existence of DNA G4s is well established, the presence of folded G4 structures in RNA has proven to be controversial, with some studies confirming their existence (12) and others providing evidence that they are globally unfolded *in vivo* (13). However, RNA G4s have been implicated in inhibiting translation (14,15) or modulating telomere structure and function (16) and can be targeted by small molecules (17).

*To whom correspondence should be addressed. Tel: +1 301 228 4620; Fax: +1 301 846 6033; Email: schneeklothjs@mail.nih.gov

By targeting G4s with small molecules, it is possible to control the expression of otherwise 'undruggable' oncogenic proteins, such as KRAS. KRAS, a prototypical oncogene, encodes for a small GTPase that influences cell growth and apoptosis (18). Single point mutations, commonly at codons 12, 13 or 61, cause KRAS to be constitutively active and trigger oncogenesis. Consequently, these mutations are found in a wide variety of tumors. While KRAS is an attractive drug target, small molecules that perturb the function of the KRAS protein are exceedingly rare due to its small size and lack of 'druggable' pockets (19). However, a G4 in the *KRAS* promoter has recently been demonstrated to regulate transcription of the gene. The structure of the quadruplex in the *KRAS* promoter is polymorphic, with most conformations containing an atypical single nucleotide bulge (18). A structure of a G4-forming sequence derived from the *KRAS* promoter was recently solved by NMR, confirming the proposed structure (20). Previous studies have provided preliminary evidence that the *KRAS* G4 can indeed be targeted with small molecules to elicit changes in KRAS expression (21–23). A longstanding goal has been to develop selective small molecules that elicit a therapeutic response by binding to specific G4 structures (24). CX-5461, currently in phase I clinical trials, targets BRCA1/2 deficient tumours, and is suspected to act by stabilizing multiple G4s though it also stabilizes dsDNA (25). Quarfloxin (CX-3552, Cylene Pharmaceuticals, Tetragene), is reported to inhibit rRNA biogenesis by the disruption of the interaction between nucleolin and ribosomal G4 DNA. Quarfloxin was the first G4-stabilizing molecule to advance to clinical trials, however it did not proceed past phase II trials (26). G4-targeting drugs remain the focus of significant clinical investigation (11,27).

With a few exceptions (28), approaches that profile the binding properties of small molecules to classes of similarly structured nucleic acids are lacking. Most efforts to identify G4-binding molecules to date have focused on only screening an individual G4 and provide little information regarding selectivity (29). Recent advances indicate that drug-like small molecules can form highly selective interactions with DNA (30) and RNA (31–34) and have effects *in vivo*. One powerful way to leverage this observation is to identify nucleic acid targets for FDA approved drugs as these molecules have already been widely used in humans. Previous approaches have investigated libraries from the NCI and collections of FDA approved drugs, and identified drugs such as methylene blue and tricyclic antidepressants as binding to G4 structures (35–37). To investigate the G4-binding properties of known drugs, we herein report the use of a small molecule microarray (SMM) screening platform to profile interactions of a chemically diverse collection of compounds (including many clinically used drugs) with different G4 structures from oncogenic promoters and mRNA. Through biochemical, structural, and biological evaluation we identify chlorhexidine, a widely clinically used oral antiseptic (38), that preferentially binds to the DNA G4 in the promoter of the *KRAS* gene and suppresses KRAS expression in cancer cells.

MATERIALS AND METHODS

Small molecule microarray screening

Small molecule microarray screening was carried out as previously described (39–40). Briefly, γ-aminopropyl silane (GAPS) microscope slides (Corning) were functionalized with a short Fmoc-protected amino polyethylene glycol spacer. After deprotection using piperidine, 1,6-diisocyanatohexane was coupled to the surface by urea bond formation to provide functionalized isocyanate-coated microarray slides that can react with primary alcohols and amines to form immobilized chemical screening libraries. A total of 3607 unique small molecule stock solutions (10 mM in DMSO) from MIPE (41) and NCI Diversity set V (42) screening collections, in addition to dyes and controls, were printed in duplicate onto one slide and exposed to pyridine vapor in a vacuum desiccator overnight to facilitate covalent attachment to the slide surface. After drying, slides were incubated with a 1:20 polyethylene glycol:DMF (v/v) solution to quench unreacted isocyanate surface. G4-forming oligonucleotides were annealed by heating to 95°C for 5 min, cooled to RT, and diluted to 500 nM in PBST with 100 mM KCl. Proper folding of each oligonucleotide was confirmed by circular dichroism spectroscopy. Next, printed slides were incubated for 2 h at RT with a 5′-AlexaFluor647-labeled G4 oligonucleotide of interest (see below for sequences used in screening). Following incubation, slides were gently washed three times for 2 min in PBST, once in deionized water, and dried by centrifugation for 2 min at 4000 rpm. Fluorescence intensity was measured (650 nm excitation, 670 nm emission) on a Innopsys Innoscan 1100 AL Microarray Scanner. Hits were identified based on signal-to-noise ratio (SNR), defined as (mean foreground − mean background)/standard deviation of background, and *Z*-score, defined as: $Z =$ (mean SNR635compound – mean SNR635library)/(SD SNR635library) with the following criteria: (i) SNR > 0, (ii) Z score > 3, (iii) coefficient of variance (CV) of replicate spots <100, (iv) SNR of negative control slide <1 and (v) visual comparison of intensity with other nucleic acid structures screened. Screens were performed in parallel with the following oligos:

- Alexafluor647-AKTIP: 5′-Alexafluor648 GGGGUG GGGCGGGGCGGGG
- Alexafluor647-BCl2: 5′-Alexafluor648 AGGGGCGG GCGCGGGAGGAAGGGGGCGGGA
- Alexafluor647-MYC: 5′-Alexafluor648 AGGGTGGG GAGGGTGGGG
- Alexafluor647-MYB: 5′-Alexafluor648 GGAGGAGG AGGTCACGGAGGAGGAGGAGAAGGAGGAGG AGGA
- Alexafluor647-RB1: 5′-Alexafluor648 CGGGGGGTTT TGGGCGGC
- Alexafluor647-VEGF: 5′-Alexafluor648 CGGGGCGG GCCGGGGGCGGGGT
- Alexafluor647-c-KIT: 5′-Alexafluor648 AGGGAGGG CGCTGGGAGGAGGG
- Alexafluor647-KRAS: 5′-Alexafluor648 AGGGCGGT GTGGGAAGAGGGAAGAGGGGGAGGCAG

Thermal melt assay

The thermal stability of the *KRAS* oligonucleotide (AGGG CGGTGTGGGAAGAGGGAAGAGGGGGAGGCAG) in the presence and absence of compound was determined using an Aviv Biomedical Model 420 Circular Dichroism (CD) Spectrometer equipped with a ThermoCube temperature regulator. To anneal the oligonucleotide, the sample was heated to 95°C for three minutes and allowed to cool to room temperature upon standing over the course of 1–2 h. The oligonucleotide was then diluted to a final concentration of 10 μM in 10 mM Tris buffer (pH 6.6, containing either 30 mM KCl or 100 mM KCl) and four equivalents of compound were added to yield 40 μM compound in 1% DMSO. The buffer contained 30 mM KCl when evaluating measuring the *KRAS* G4 melting temperature with CLX, ALX and PG. The buffer contained 100 mM KCl when measuring the panel of oligonucleotides with CLX, except for *HIF1α* and dsDNA, which had 30 mM KCl. Spectra were recorded from 224 to 312 nm at 25°C with a step size of 2 nm, followed by heating from 25 to 97°C at 1°C/min in a 0.1 cm quartz cuvette. To calculate the T_m of each sample, ellipticity was plotted as a function of temperature and fit in GraphPad Prism 7 software using a nonlinear sigmoidal dose–response model with a variable slope. Each experiment was performed in triplicate, with ΔT_m values calculated using T_m(+compound) – T_m(–compound) and then averaged to yield the final value. The following oligos were used in these experiments:

- KRAS: 5′-AGGGCGGTGTGGGAAGAGGGAAG AGGGGGAGGCAG
- MYC: 5′-AGGGTGGGGAGGGTGGGG
- dsDNA: 5′-CAATCGGATCGAATTCGATCCGATT G
- RB1: 5′-CGGGGGGTTTTGGGCGGC
- VEGF: 5′-CGGGGCGGGCCGGGGGCGGGGT
- c-KIT: 5′-AGGGAGGGCGCTGGGAGGAGGG
- BCL-2: 5′-AGGGGCGGGCGCGGGAGGAAGGG GGCGGGA
- HIF1α: 5′-GGGAGGGAGAGGGGGCGGG

Fluorescence intensity titration

Alexa Fluor 647-labeled *KRAS* (5′A647-AGGGCGG TGTGGGAAGAGGGAAGAGGGGGAGGCAG-3′) was heated at 95°C for 3 min, allowed to cool to room temperature, and diluted to 50 nM in 25 mM Tris buffer (pH 6.4, containing 50 mM KCl). Compound was added as a solution both in buffer containing 2–3% DMSO, and the sample was allowed to equilibrate for 10 min. Fluorescence intensity spectra were recorded at room temperature using a Photon Technology International, Inc. QuantaMaster 600™ Spectrofluorometer equipped with Felix GX 4.2.2 software. Fluorescence intensity was recorded at an excitation wavelength of 645 nm, with the resulting emission spectrum recorded from 650 to 800 nm, and the fluorescence intensity at the emission maximum was used in all calculations.

NMR

All NMR spectra were recorded at 293 K on a Bruker AVANCE III 500 MHz spectrometer equipped with a TCI cryoprobe. NMR buffer was composed of 25 mM Tris-d_{11} (pH 6.6, containing 50 mM KCl) in 100% H_2O, and subsequently prepared NMR samples contained 10% DMSO-d_6 to improve compound solubility. The ^{13}C-labeled chlorhexidine was first dissolved in a 10 mM stock concentration, and then added to the NMR buffer, and a carbon NMR was performed. Next, the *KRAS* oligonucleotide (AGGGCGGTGTGGGAAGAGGGAAGAGG GGGAGGCAG) was buffer exchanged (3 kDa MWCO spin column, EMD Millipore) into the NMR buffer and added to the sample. A second carbon NMR was performed. All data were processed and visualized with MestReNova software (Version 8.1.2-11880).

All ligands were first dissolved in DMSO-d_6 to a 20 mM stock concentration, and *KRAS* oligonucleotide (AG GGCGGTGTGGGAATAGGGAA (20)) was buffer exchanged (3 kDa MWCO spin column, EMD Millipore) into the NMR buffer. For the chlorhexidine titration, the buffer was subsequently prepared containing 10% D_2O and 5% DMSO-d_6. For alexidine and proguanil titrations the buffer was prepared containing 10% DMSO-d_6 to account for differing solubility. For all 1D-^{1}H NMR titrations, ligands were diluted to their respective NMR buffer to 1 mM, and titrated into 100 μM *KRAS* G4 in NMR buffer. For WaterLOGSY experiments, a reference 1D-^{1}H and 1D WaterLOGSY spectrum of 100 μM *N*-methyl-L-valine and 100 μM compound was collected, followed by a separate sample containing 1 μM *KRAS*, 100 μM *N*-methyl-L-valine, and 100 μM compound. All 1D-^{1}H NMR spectra were recorded using the 'zgesgp' excitation sculpting water suppression pulse sequence from Bruker, with 128 scans (43). All data were processed and visualized with MestReNova software (Version 8.1.2-11880).

Water-ligand observed via gradient spectroscopy (WaterLOGSY) NMR

A reference 1D-^{1}H and 1D WaterLOGSY spectrum of 100 μM *N*-methyl-L-valine and 100 μM compound was collected, followed by a separate sample containing 1 μM KRAS oligo, 100 μM *N*-methyl-L-valine, and 100 μM compound. A shortened KRAS oligonucleotide (AGGGCGGT GTGGGAATAGGGAA (20)) was buffer exchanged into 25 mM Tris-d_{11} buffer (pH 6.6, containing 50 mM KCl) using centrifugal filtration (3 kDa MWCO, EMD Millipore). A sample of chlorhexidine (Sigma Aldrich) and *N*-methyl-L-valine (Chem-Impex-International), each at 100 μM, was prepared in 25 mM Tris-d_{11} buffer (pH 6.6, containing 50 mM KCl and 10% DMSO-d_6), and 1D reference proton and WaterLOGSY spectra without oligonucleotide were recorded. NMR spectra were recorded at 293 K on a Bruker AVANCE III 500 MHz spectrometer equipped with TCI cryoprobe.

Surface plasmon resonance (SPR)

SPR was conducted using a Biacore 3000 (Biacore, Inc.) instrument. NeutrAvidin (ThermoFisher) was im-

mobilized to 20 000 RU in both flow cells using EDC/NHS coupling to a CM5 chip (GE). The surface was then blocked with ethanolamine. Next, 1 μM 5′-biotin-TEG AGGGCGGTGTGGGAAGAGGGAAGAGGGG GAGGCAG (obtained as an HPLC-purified sample from Integrated DNA Technologies, Inc.) was refolded in 10 mM Tris, 30 mM KCl, 3% DMSO, pH 6.6 by heating at 95°C in a heater block for three minutes then cooled to room temperature, and immobilized on one flow cell of the SPR chip to a density of 450 RU. Compounds were injected at a flow rate of 30 ml/min in 10 mM Tris, 30 mM KCl, 3% DMSO, 0.01% Tween-20, pH 6.6 for 1 min. Each injection was repeated twice for consistency. Each trace was fit individually to a Langmuir model for chlorohexidine. Alexidine was fit to a steady state model (44). No binding was observed for proguanil.

Cell culture and viability

MDA-MB-231 cells were purchased from ATCC and were maintained at 37°C with an atmosphere of 5% CO_2 in DMEM supplemented with 10% fetal bovine serum, 2 mM L-glutamine, 100 IU/ml penicillin and 0.1 mg/ml streptomycin. For confluence measurements, cells were seeded into 96-well plates at 5000 cells/well and allowed to attach overnight. The following day media was removed and fresh media (100 μl) containing compound or DMSO (0.1% final) added to each well. Cells were incubated at 37°C and monitored every hour for at least 24 h by IncuCyte® ZOOM Live-Cell Analysis System (Essen BioScience). Additionally, cell viability was measured using an MTT assay. Following incubation with compound, media was removed and MTT solution (1.2 mM in growth media) added to each well (100 μl). Cells were incubated at 37°C for 2 h, after which time the media was removed, cells were washed with PBS (100 μl), and DMSO (50 μl) added with mixing. The absorbance was measured at 570 nm using a BioTek Synergy 2 Microplate Reader and data were normalized to DMSO controls.

Human multiple myeloma cell line KMS-28BM was cultured in Advanced RPMI 1640 (6% heat-inactivated fetal bovine serum (FBS): Gibco by Life Technologies, 2 mM L-glutamine: Gibco by Life Technologies, 100 U/ml Penicillin and 100 μg/ml Streptomycin: Gibco by Life Technologies, 100 ug/ml Normocin: InvivoGen) and incubated at 37°C with 5% CO_2. Media was changed every two days. For cells plated and harvested for protein or RNA, pellets were washed twice with cold PBS. After aspirating off the PBS, pellets were flash frozen in dry ice and transferred to a −80°C freezer for short term storage. Cell viability experiments were performed using CellTiter 96 AQueous One Solution Cell Proliferation Assay System (Promega). Cells were plated in quadruplicate on clear, flat-bottomed 96-well tissue cultured treated plates (Corning Costar) and incubated for each designated time in a 37°C incubator with 5% CO_2. Concentrated drug stocks were diluted down in Eppendorf tubes to each specific dose point before being added to the plate. After incubation, MTS reagent was added directly to the wells and incubated again at 37°C with 5% CO_2 for 90 min. The absorbance of the MTS formazan was immediately read at 500 nm on an Omega 640 spectrophotometer. A blank measurement was taken from the absorbance of the wells with media only and subtracted accordingly. Percentage cell viability was normalized to the absorbance of untreated wells after blanking and averaged from the four quadruplicate wells.

Western blots

MDA-MB-231 cells were seeded into six-well plates at 250 000 cells/well and allowed to grow for 24 h. Day-old media was removed and cells were incubated with compounds or DMSO (0.1% final) in fresh media for 48 or 72 h. Following incubation, cells were washed with PBS (3 × 1 ml) then lysed by the addition of cold RIPA buffer (150 μl) supplemented with 6 M urea and 1X Halt™ protease and phosphatase inhibitor cocktail with EDTA (ThermoFisher). Samples were homogenized by passing several times through a 22G needle and centrifuged to clear. Protein concentration was determined by Qubit™ Assay (ThermoFisher) or using a NanoDrop 2.0 Spectrophotometer. Equal amounts of protein were loaded onto NuPAGE 4–12% Bis–Tris Protein Gels (ThermoFisher), resolved by electrophoresis, and transferred to nitrocellulose membranes for western blot analysis with anti-RAS antibody (610002, BD Transduction Labs) and anti-actin antibody (MAB1501R, EMD Millipore). Blots were visualized by chemiluminescence with LumiGLO® Reagent (Cell Signaling Technology) and an ImageQuant LAS 4000 (GE Life Sciences) imaging system.

KMS-28BM cell pellets were first lysed in RIPA buffer (RIPA, sodium orthovanadate, PMSF, protease inhibitor, and phosphatase inhibitors A and B), vortexed to homogenize, and sonicated in an ice water bath for 5 min on high, with intervals of 30 s on, 1 min off. Homogenized pellets were then incubated on ice for 90 min before spun down and transferred to new Eppendorf tubes. Protein was next quantitated by a standard BCA protocol. 15 μg of protein was loaded into each well of 4–12% Bis–Tris Gels (Novex), electrophoresed at 135 V for 90 min to achieve optimal band separation, and transferred with the iBlot2 system (Life Technologies). Equal protein loading and transfer was confirmed by Ponceau staining (Thermo Scientific) after the initial protein transfer. Western blots were blocked in 5% dry milk in 1× TBST (10× TBS, DI H_2O, Tween 20) for 1 h, washed three times in 1× TBST for 10 min each, and incubated on a rocker in a 4°C cold room overnight with primary monoclonal antibodies in 5% BSA at the designated dilution by the manufacturer. Blots were washed three times with 1× TBST before incubation with the appropriate species and dilution of polyclonal secondary antibodies in 5% dry milk on a rocker at room temperature for 1 h. Blots were again washed three times with 1× TBST before imaging with SuperSignal West Dura Chemiluminescent Substrate (Thermo Scientific) on a GBOX F3 Imager (Syngene).

KRAS transfection

MDA-MB-231 cells were seeded into 24-well plates at 125 000 cells/well and allowed to attach overnight. Plasmid DNA was transfected into cells using Lipofectamine LTX with PLUS Reagent (15338030, ThermoFisher) according

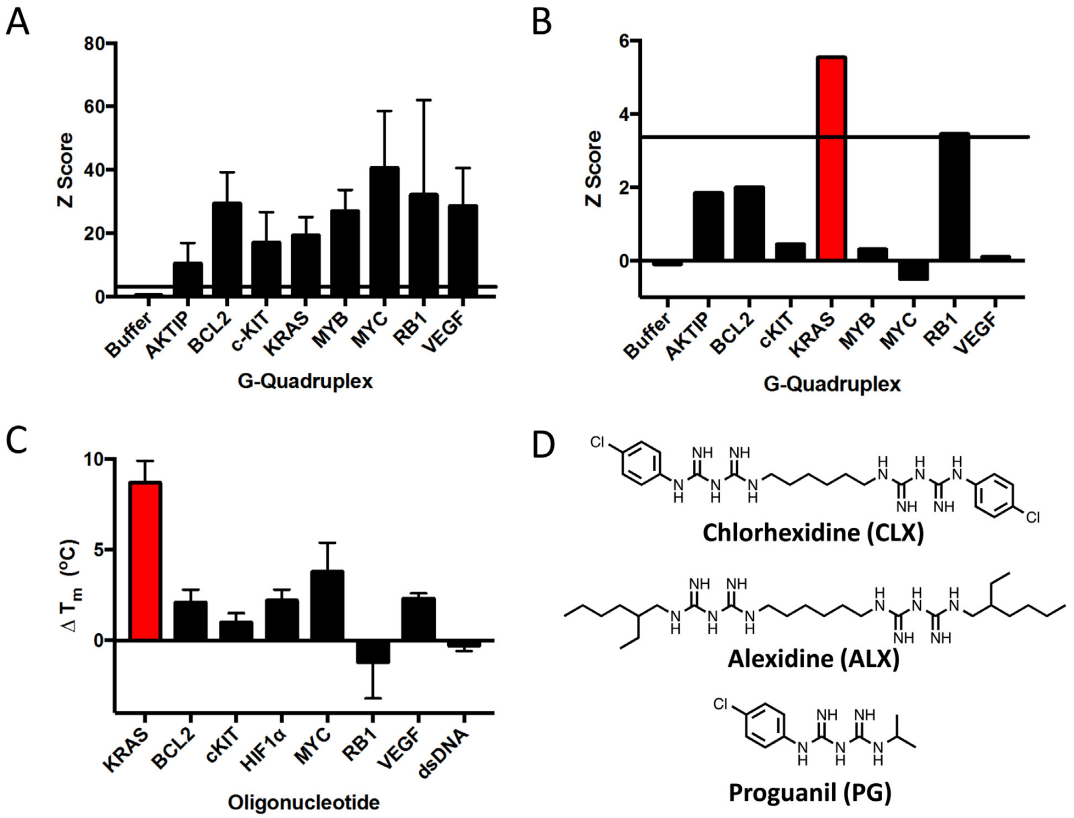

Figure 1. SMM Z score of G4s binding to (**A**) pyridosatin and (**B**) CLX. Horizontal line corresponds to 'hit' cutoff of 3. (**C**) Increase in melting temperature of a panel of G-quadruplexes in the presence of four equivalents of CLX (measured by circular dichroism). (**D**) Chemical structures of Chlorhexidine (top), Alexidine (middle) and Proguanil (bottom).

to the recommended protocols. Briefly, plasmid DNA was diluted in Opti-MEM Reduced Serum Media (0.5 μg DNA in 100 μl media, per well) and PLUS Reagent (0.5 μl) added. The solution was mixed and incubated at room temperature for 10 min, after which Lipofectamine LTX Reagent (1.5 μl) was added, mixed and incubated at room temperature for another 30 min. Growth media was removed from cells and replaced with Opti-MEM, then DNA-lipofectamine complexes (100 μl) were added with gentle mixing. Cells were incubated at 37°C for 4 h, then Opti-MEM media was removed and replaced with complete growth media containing compound or DMSO (0.1% final) and incubated at 37°C for 48 h. Following incubation, cells were lysed and KRAS levels were analyzed by western blot as described above using an anti-HA antibody (715500, ThermoFisher). The KRAS plasmid (pCDH-CMV-HA-KRAS4BG12V-EF1-puro) was kindly provided by Deborah Morrison (Center for Cancer Research, National Cancer Institute).

RESULTS

SMM profiling to identify nucleic acid interacting drugs

To probe nucleic acid binding to known, pharmacologically active compounds, we used an SMM screening platform (40,45). We generated SMMs consisting of the MIPE library (41,46,47) (a collection of 1902 FDA approved drugs, compounds currently undergoing clinical trials, and other well-annotated and validated inhibitors) and the NCI Diversity set (42) (a freely available collection of 1705 chemically diverse compounds). We then incubated each array in parallel with eight different fluorescently labeled G4 structures derived from oncogenic promoters (*MYC* (48), *KRAS* (49), *MYB* (50), *c-KIT* (51), *BCl2* (52), *RB1* (53), and *VEGF* (54)) or mRNA (*AKTIP* (14)). For each compound, a composite *Z*-score was calculated based on increased fluorescence at that location on the array in the presence of a given oligonucleotide. Compounds with a *Z*-score greater than three were considered 'hits' worthy of further investigation. The average hit rate for a G4 was 0.92%, and 2.9% of the compounds were scored as hits for at least one G4. It should be noted that this library contains a somewhat high proportion of compounds containing reactive functional groups such as nitrogen mustards, other alkylating functionalities, and polycationic scaffolds. Thus, this collection is slightly more likely to contain 'hits' through promiscuous interactions than more traditional libraries previously screened in this format. In fact, most hit compounds bound to many G4 structures, highlighting the challenge of specificity in targeting G4s. As one example, the polycationic aminoglycoside tobramycin was found to bind nearly every G4 structure investigated in the screen. In a separate experiment, we evaluated pyridostatin, a well-validated pan-G4 binding molecule, which was not included in the original library (55). Pyridostatin strongly bound to every G4 oligo evaluated, confirming both the binding of this molecule to G4

structures in the SMM format and the proper folding of G4 oligos under screening conditions (Figure 1A).

A small number of compounds had high *Z*-scores for individual G4s, resulting in binding profiles consistent with more selective interactions. Of particular interest was the bisbiguanide drug chlorhexidine (CLX), an oral disinfectant and component of prescription mouthwash (56), which preferentially bound to the G4 from the *KRAS* promoter (Figure 1B). Previous studies have demonstrated that compounds that increase the thermal stability of G4 structures can profoundly affect gene expression (24). To assess the stabilization effects and selectivity of CLX, we performed thermal melt assays measured by circular dichroism (CD) on known quadruplexes, some evaluated in the SMM, as well as dsDNA, in the presence of 100 mM KCl with excess CLX. CLX had no effect on the melting temperature of dsDNA, indicating that it is selective for G4 structures over duplex DNA. In comparison to the *KRAS* G4, CLX also had weaker or no effect in thermal melt assays for all other quadruplexes investigated, aligning with the selectivity profile observed in the initial SMM profiling (Figure 1C).

Biophysical characterization of the CLX/*KRAS* G4 interaction

While investigating the interaction of CLX with the *KRAS* G4, we also studied alexidine (ALX), a structurally related drug that is also primarily used as an antiseptic in clinical settings (Figure 1D) (56). Both CLX and ALX have been reported to exert anticancer effects through inhibition of protein-protein interactions, such as between Bcl-x_L and Bak (57). We also investigated proguanil (PG), a structurally related monomeric biguanide drug that is used as an antimalarial agent (Figure 1D) (56). We pursued a series of structural, biochemical, and biological assays to evaluate the interactions of CLX, ALX and PG with the *KRAS* G4. First, as measured by CD, with 30 mM KCl the melting temperature of the *KRAS* G4 increased considerably in the presence of CLX ($\Delta T_m = 13.0 \pm 0.7$ °C) demonstrating binding and stabilization. ALX induced moderate stabilization ($\Delta T_m = 7.1 \pm 0.6$ °C), while PG did not change the melting temperature of the G4. By comparison, under these conditions pyridostatin had a ΔT_m of 31.6 ± 2.6 °C, consistent with observations that it is both a tighter and less specific G4 binder (Supplementary Figure S1). Next, a fluorescence titration assay was used to gain a more quantitative perspective of interactions between biguanide drugs and G4 structures. Compounds were titrated into a solution of 5′-AlexaFluor647-labeled *KRAS* G4, fluorescence was monitored as a function of compound concentration, and K_D values were derived from changes in fluorescence. In this assay, CLX had the tightest affinity ($K_D = 5.5 \pm 2.9$ μM) (Figure 2B), ALX had weaker affinity ($K_{Dapp} = 19.3 \pm 11.0$ μM), and PG induced only minimal changes in fluorescence intensity ($K_{Dapp} > 200$ μM) (Supplementary Figure S2). Subsequently, surface plasmon resonance (SPR) studies were pursued. These experiments confirmed a reversible and saturable interaction between CLX and the

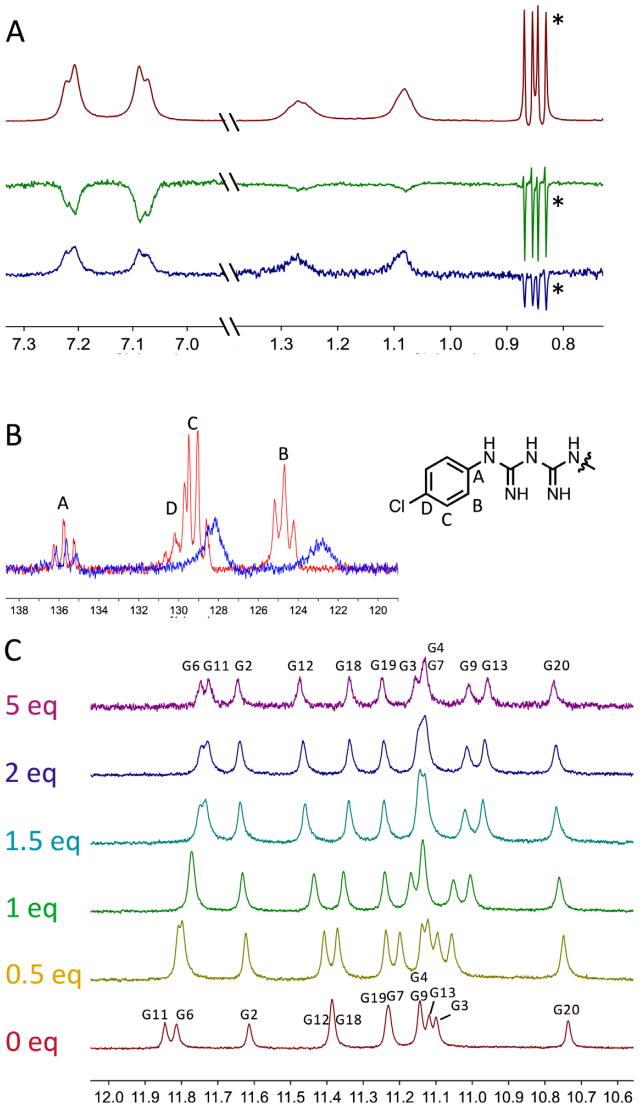

Figure 2. (**A**) ^{1}H NMR of CLX and *N*-methyl-L-valine (non-binding control, peaks indicated with *) (Top), WaterLOGSY NMR of CLX and *N*-methyl-L-valine in the absence (middle) and presence (bottom) of *KRAS* G4. (**B**) ^{13}C NMR of ^{13}C-labeled CLX in the absence (red) and presence (blue) of *KRAS* G4. (**C**) ^{1}H NMR of imino peaks of *KRAS* G4 in the presence of 0–5 eq of CLX.

Table 1. Biophysical analysis of CLX, ALX, and PG binding to the *KRAS* G4

Compound	ΔT_m (°C)	K_D (μM), FIA	K_D (μM), SPR
CLX	13.0 ± 0.7	5.5 ± 2.9	1.1 ± 0.5
ALX	7.1 ± 0.6	19.3 ± 11.0[a]	12.1 ± 0.5[a]
PG	<1	>200[a]	>20[b]

[a] K_D apparent.
[b] No binding observed at 20 μM.

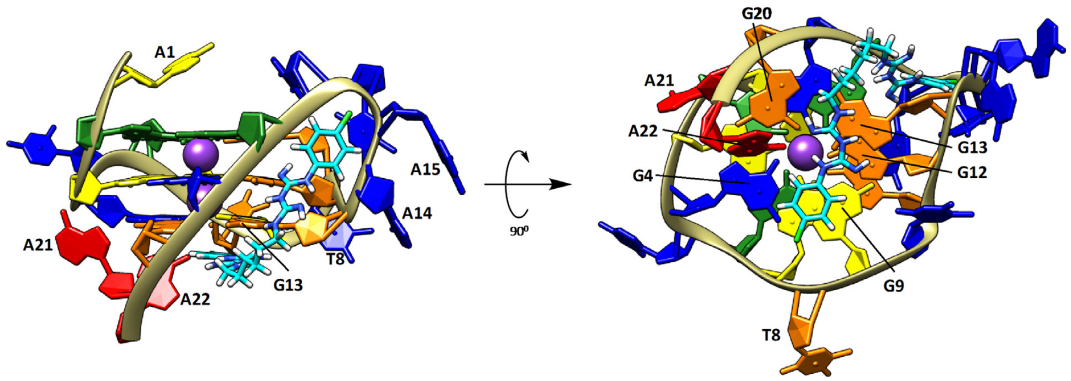

Figure 3. Structure of *KRAS* G4 (PDB: 5I2V). Nucleic acids are colored based on magnitude of chemical shift perturbations of H8/H6 protons in the presence of 1 eq of CLX: 0–0.020 Δδ ppm (blue), 0.020–0.035 Δδ ppm (green), 0.035–0.050 Δδ ppm (yellow), 0.050–0.080 Δδ ppm (orange), >0.080 Δδ ppm (red). Indicated binding site for CLX (cyan) is the most consistent with chemical shift perturbations and docking studies.

KRAS G4 (K_D = 1.1 ± 0.5 μM) (Figure 2C). ALX had a more complex sensorgram, consistent with a less specific mode of interaction with the G4, and kinetic methods were not suitable for analysis (Supplementary Figure S3). However, using a steady state method, the affinity was approximated to be weaker than that of CLX (K_{Dapp} = 12.0 ± 0.5 μM). Finally, PG did not bind under any conditions tested (see Supplementary Figure S3). These results were in good agreement with the fluorescence titration and thermal melt assays, where CLX had the highest affinity and was the most stabilizing compound (Table 1).

NMR studies indicate a binding site for CLX on the *KRAS* G4

To gain more insight into the interaction of CLX with the *KRAS* G4, a series of NMR experiments were pursued. First, we performed WaterLOGSY experiments using *N*-methyl-L-valine as an internal, non-binding control to confirm that CLX did not aggregate in solution and bound the *KRAS* G4 (Figure 2A). Due to significant line broadening in the presence of DNA, ligand-observed ^{1}H chemical shift perturbation experiments were unsuccessful. To circumvent this problem, we prepared an isotopically enriched sample of CLX where all aromatic carbons were ^{13}C labeled (Scheme S1). In ^{13}C NMR experiments using the labeled CLX sample, both chemical shift perturbations and line broadening were observed in three of the four aromatic carbons in the presence of the *KRAS* G4, highlighting the role of the aromatic group in G4 recognition (Figure 2B). In contrast, carbons directly bonded to the biguanide groups were only minimally perturbed.

Next, a titration of unlabeled CLX into *KRAS* G4 DNA confirmed that chemical shift perturbations of DNA peaks occurred in the presence of CLX (Figure 2C). Peaks were assigned based on previously reported data (PDB: 5I2V) (20) and confirmed by NOESY analysis both before and after CLX addition. Chemical shift perturbations were observed in both the imino and aromatic regions of the *KRAS* G4 (Figure 2C and Supplementary Figure S5). Perturbations saturated before two equivalents of CLX were added, providing evidence for the formation of a 1:1 complex, in contrast to the 2:1 complexes seen with other G4 ligands (41). C/T H6 and G/A H8 aromatic and imino proton shifts were quantified and mapped onto the structure of the G4 (Supplementary Figures S6 and S7). In both cases, chemical shifts were clustered near G11, G12, G13, A21 and A22, indicating a possible binding site. Only chemical shift perturbations were observed in the loop regions, including the highly flexible A14-A17 loop. However, the T8 bulge showed a comparatively large perturbation. Additional titration experiments with ALX and PG confirmed moderate or weak, nonspecific binding interactions, respectively (Supplementary Figures S9 and S10), highlighting that subtle differences in the biguanide compounds' chemical structure significantly impact binding events.

We next evaluated the CLX–*KRAS* G4 interaction with computational docking simulations using ICM modelling software (ICM version 3.8–4a). Using residues that showed chemical shift perturbations by NMR to define a receptor site, we docked CLX to all 10 of the available low energy conformations of the *KRAS* G4 (PDB: 5I2V). The ten lowest energy CLX–*KRAS* binding interactions showed two plausible binding regions on the *KRAS* G4, one of which is more consistent with the observed chemical shift perturbations (Figure 3). Both potential interactions involve CLX binding to the grooves of the *KRAS* G4, which is a known but less common binding mode (58,59) than the stacking interactions most commonly seen with G4 ligands (48,60–62). Additionally, we utilized the PocketFinder module available through this software to analyze potential small molecule binding pockets on the G4 structure. This analysis indicated four potential sites where small molecules could plausibly interact with the G4, two of which are occupied by the CLX binding conformation shown (Figure 3, Supplementary Figure S11). These modelling studies suggest a possible binding mode in which the aromatic rings in CLX stack with nucleobases in the G4 and are consistent with the observation that ALX has a weaker interaction.

Effects of CLX on KRAS expression and toxicity in cancer cells

Next, the toxicity of CLX was evaluated across a panel of 59 different cancer cell lines. Cell lines with mutations in KRAS strongly correlated with increased sensitivity toward

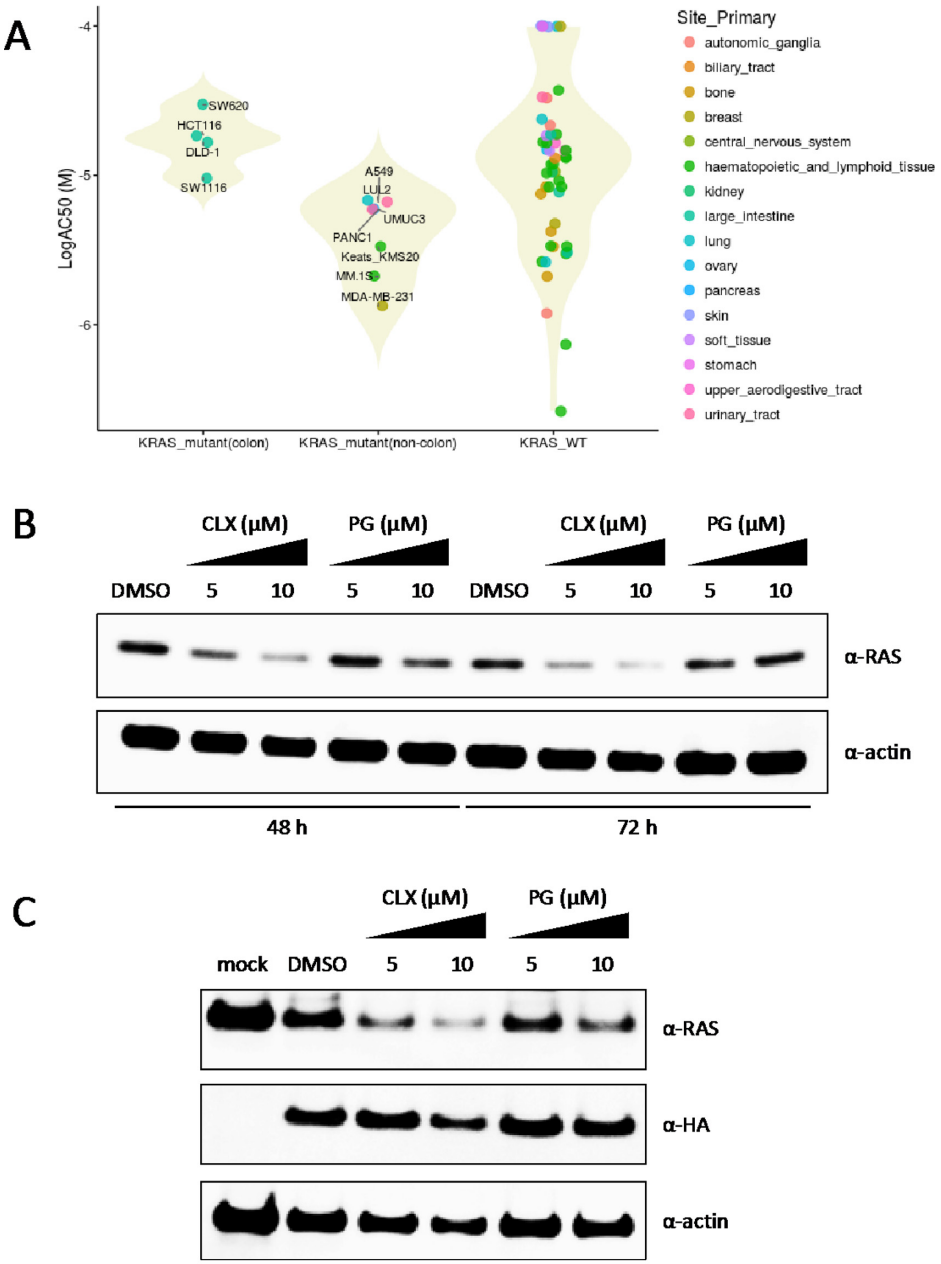

Figure 4. (**A**) Comparison of CLX activities across a panel of cancer cell lines from viability assay. The violin plot summarizes the distribution of $\log_{10}(AC_{50})$ grouped by their respective KRAS mutational status and primary site. The *P*-values are calculated using Student's *t*-test. (**B**) Western blot analysis of KRAS protein levels in MDA-MB-231 cells after 48 and 72 h of treatment with CLX or PG. (**C**) Western blot analysis of MDA-MB-231 cells transiently transfected with HA-tagged KRAS plasmid (lacking a G4) and dosed with CLX or PG for 48 h.

CLX (*P*-value = 0.007 ($KRAS_{mut\text{-}noncolon}$ versus $KRAS_{wt}$)) (Figure 4A, Supplementary Figure S12). The notable exception to this trend was colorectal cancers, which did not display increased sensitivity (*P*-value = 0.4 ($KRAS_{mut\text{-}colon}$ versus $KRAS_{wt}$)). Of note, unlike many other cancers KRAS mutations are not suspected to initiate colorectal cancers (63). We validated CLX-mediated effects on KRAS expression in the MDA-MB-231 breast cancer cell line, where KRAS harbors an oncogenic G13D mutation, the most sensitive cell line with a KRAS mutation. After treatment for 48 h with CLX, EC_{50} values of 5.7 and 4.3 μM were found in MDA-MB-231 cells by MTT assay and confluence measurements, respectively (Supplementary Figure S13). In contrast, PG was not toxic (EC_{50} > 20 μM). Treatment with CLX for 48 and 72 h also resulted in a marked decrease in KRAS protein levels as determined by Western blot, while PG had no effect on the expression of KRAS at 72 h (Figure 4B). In contrast, when MDA-MB-231 cells were transiently transfected with an HA-tagged *KRAS* plasmid driven by the CMV promoter (which lacks a G4 in its promoter), treatment with CLX showed no suppression of the HA-tagged KRAS protein by Western blot. However,

native KRAS levels in the same cells were still significantly decreased upon CLX treatment (Figure 4C). Thus, a KRAS gene controlled by a promoter lacking a G4 element is not affected by CLX treatment. For a second, representative cell line, we investigated KMS-28BM, a multiple myeloma cell line, harbouring a G12A KRAS oncogenic mutation. Treatment with CLX resulted in a similar decrease in KRAS protein (Supplementary Figure S14B).

DISCUSSION

We have used an SMM screening and profiling approach to identify FDA approved drugs that interact with G4 structures in oncogene promoters. As part of an in-depth validation, we confirmed that CLX and the structurally related ALX bind the *KRAS* G4. CLX, but not the structurally related drug PG, decreased KRAS expression though a G4-driven mechanism, corresponding with decreased levels of KRAS protein. Importantly, these compounds have a discrete structure-activity relationship associated with binding to G4 structures. CLX, a bisbiguanide containing two aromatic groups, binds via a specific interaction, likely supported by π-stacking with the G4 nucleotides. ALX, an alkyl-substituted bisbiguanide, had a more complex interaction that appears to be less specific. In contrast, PG, a similar, monomeric biguanide drug, exhibited weak or no binding. A series of NMR experiments confirmed that CLX interacted directly with the *KRAS* G4 and pointed toward a distinct binding site, which was further supported by computational docking simulations. Importantly, PG had minimal effects in biochemical and biological assays, implying that two biguanide functional groups are necessary for a binding event that elicits a biological response.

Bisbiguanide antiseptics are widely used in prescription antibacterial mouthwash and are considered essential medicines by the World Health Organization (64). Furthermore, these compounds have been demonstrated to inhibit protein-protein interactions, particularly related to Bcl-x_L, and to have anticancer activity (57). The work reported here suggests that CLX and related compounds may also influence gene expression by interacting with G4 nucleic acid structures in oncogene promoters. Thus, CLX should be considered to have a pleiotropic mechanism of action, most likely interacting with many targets in the cell. Importantly, the typically administered dose of CLX (0.2–2% by weight) (65) is above the concentrations required to induce changes in gene expression and lower than the 18–21 μM concentration required to inhibit protein-protein interactions (57).

The work reported here suggests that more efforts evaluating the anticancer effects of chlorhexidine may be warranted. Given the wide usage of CLX in prescription mouthwashes, it would be of particular interest to evaluate CLX against head and neck cancers, particularly oral cancers. In fact, others have already shown that bisbiguanide antiseptics have some anticancer effects in several oral cancer cell lines (57). While the activity was attributed to inhibition of protein-protein interactions, our work suggests that G4 binding might also be a (potentially synergistic) mechanism of action, in addition to the widely accepted ability of CLX to perturb membranes. The multiple mechanisms of action of CLX means that it can be highly cytotoxic to many cell types in culture at higher concentrations. For example, toxicity to fibroblasts in culture is observed once the concentration of CLX surpasses ~100 μM (66), a commonly clinically used concentration.

More broadly, the SMM screening and profiling approach appears to be a useful method both to investigate nucleic acid targets for known drugs and to provide evidence for their binding specificity. This work also suggests that it may be worthwhile to consider nucleic acid-binding events when studying off-target pharmacology in drug discovery. Moving forward, identifying nucleic acid targets for other FDA approved drugs may be a fruitful and largely unexplored way to repurpose drugs. Studies evaluating a broader array of DNA and RNA structures using this platform are currently underway.

DATA AVAILABILITY

Genome Maps is an open source collaborative initiative available in the GitHub repository (https://github.com/compbio-bigdata-viz/genome-maps).

SUPPLEMENTARY DATA

Supplementary Data are available at NAR Online.

ACKNOWLEDGEMENTS

We thank members of the Chemical Biology Laboratory for helpful comments and suggestions including Dr J. Barchi for help with the WaterLOGSY experiments. The KRAS plasmid (pCDH-CMV-HA-KRAS4BG12V-EF1-puro) was kindly provided by Deborah Morrison (Center for Cancer Research, National Cancer Institute). We thank Dr. S. Tarasov and M. Dyba (Biophysics Resource, SBL, NCI at Frederick) for assistance with HRMS studies.

FUNDING

Division of Preclinical Innovation, National Center for Advancing Translational Sciences, Intramural, Research Program of the National Institutes of Health, Center for Cancer Research, and the National Cancer Institute (NCI), National Institutes of Health [1 ZIA BC011585 to J.S.S., 1 ZIA BC011065 for B.M.]. Funding for open access charge: Dr Schneekloth will pay for the publication charges from his budget through the National Cancer Institute.
Conflict of interest statement. None declared.

REFERENCES

1. Gottesfeld,J.M., Neely,L., Trauger,J.W., Baird,E.E. and Dervan,P.B. (1997) Regulation of gene expression by small molecules. *Nature*, **387**, 202–205.
2. Janssen,S., Durussel,T. and Laemmli,U.K. (2000) Chromatin opening of DNA satellites by targeted sequence-specific drugs. *Mol. Cell*, **6**, 999–1011.
3. Demeunynck,M., Bailly,C. and Wilson,W.D. (2003) *Small Molecule DNA and RNA Binders: From Synthesis to Nucleic Acid Complexes*. Wiley-VCH, Weinheim.

4. Shin,Y.J., Kumarasamy,V., Camacho,D. and Sun,D. (2015) Involvement of G-quadruplex structures in regulation of human RET gene expression by small molecules in human medullary thyroid carcinoma TT cells. *Oncogene*, **34**, 1292–1299.
5. Gunaratnam,M., Cuenca,F., Beltran,M., Swank,S., Fletcher,J. and Neidle,S. (2007) Targeting imatinib-resistant gastrointestinal stromal tumors by down-regulation of KIT gene expression with quadruplex-stabilizing small molecules. *Mol. Cancer Ther.*, **6**, 3519s.
6. Han,Y.W., Matsumoto,T., Yokota,H., Kashiwazaki,G., Morinaga,H., Hashiya,K., Bando,T., Harada,Y. and Sugiyama,H. (2012) Binding of hairpin pyrrole and imidazole polyamides to DNA: relationship between torsion angle and association rate constants. *Nucleic Acids Res.*, **40**, 11510–11517.
7. Swalley,S.E., Baird,E.E. and Dervan,P.B. (1997) A pyrrole-imidazole polyamide motif for recognition of eleven base pair sequences in the minor groove of DNA. *Chem.-Eur. J.*, **3**, 1600–1607.
8. Burge,S., Parkinson,G.N., Hazel,P., Todd,A.K. and Neidle,S. (2006) Quadruplex DNA: sequence, topology and structure. *Nucleic Acids Res.*, **34**, 5402–5415.
9. Hansel-Hertsch,R., Beraldi,D., Lensing,S.V., Marsico,G., Zyner,K., Parry,A., Di Antonio,M., Pike,J., Kimura,H., Narita,M. *et al.* (2016) G-quadruplex structures mark human regulatory chromatin. *Nat. Genet.*, **48**, 1267–1272.
10. Du,X.J., Wojtowicz,D., Bowers,A.A., Levens,D., Benham,C.J. and Przytycka,T.M. (2013) The genome-wide distribution of non-B DNA motifs is shaped by operon structure and suggests the transcriptional importance of non-B DNA structures in Escherichia coli. *Nucleic Acids Res.*, **41**, 5965–5977.
11. Balasubramanian,S., Hurley,L.H. and Neidle,S. (2011) Targeting G-quadruplexes in gene promoters: a novel anticancer strategy? *Nat. Rev. Drug Discov.*, **10**, 261–275.
12. Kwok,C.K., Marsico,G., Sahakyan,A.B., Chambers,V.S. and Balasubramanian,S. (2016) rG4-seq reveals widespread formation of G-quadruplex structures in the human transcriptome. *Nat. Methods*, **13**, 841–844.
13. Guo,J.U. and Bartel,D.P. (2016) RNA G-quadruplexes are globally unfolded in eukaryotic cells and depleted in bacteria. *Science*, **353**, aaf5371.
14. Agarwala,P., Pandey,S. and Maiti,S. (2014) Role of G-quadruplex located at 5 end of mRNAs. *Bba-Gen. Subjects*, **1840**, 3503–3510.
15. Kumari,S., Bugaut,A., Huppert,J.L. and Balasubramanian,S. (2007) An RNA G-quadruplex in the 5′ UTR of the NRAS proto-oncogene modulates translation. *Nat. Chem. Biol.*, **3**, 218–221.
16. Martadinata,H. and Phan,A.T. (2013) Structure of Human Telomeric RNA (TERRA): Stacking of Two G-Quadruplex Blocks in K+ Solution. *Biochemistry-US*, **52**, 2176–2183.
17. Katsuda,Y., Sato,S., Asano,L., Morimura,Y., Furuta,T., Sugiyama,H., Hagihara,M. and Uesugi,M. (2016) A Small Molecule That Represses Translation of G-Quadruplex-Containing mRNA. *J. Am. Chem. Soc.*, **138**, 9037–9040.
18. Cogoi,S. and Xodo,L.E. (2006) G-quadruplex formation within the promoter of the KRAS proto-oncogene and its effect on transcription. *Nucleic Acids Res.*, **34**, 2536–2549.
19. Dang,C.V., Reddy,E.P., Shokat,K.M. and Soucek,L. (2017) Drugging the 'undruggable' cancer targets. *Nat. Rev. Cancer*, **17**, 502–508.
20. Kerkour,A., Marquevielle,J., Ivashchenko,S., Yatsunyk,L.A., Mergny,J.L. and Salgado,G.F. (2017) High-resolution three-dimensional NMR structure of the KRAS proto-oncogene promoter reveals key features of a G-quadruplex involved in transcriptional regulation. *J. Biol. Chem.*, **292**, 8082–8091.
21. Brito,H., Martins,A.C., Lavrado,J., Mendes,E., Francisco,A.P., Santos,S.A., Ohnmacht,S.A., Kim,N.S., Rodrigues,C.M.P., Moreira,R. *et al.* (2015) Targeting KRAS oncogene in colon cancer cells with 7-carboxylate indolo[3,2-b]quinoline tri-alkylamine derivatives. *PLoS One*, **10**, e0126891.
22. Lavrado,J., Brito,H., Borralho,P.M., Ohnmacht,S.A., Kim,N.S., Leitao,C., Pisco,S., Gunaratnam,M., Rodrigues,C.M.P., Moreira,R. *et al.* (2015) KRAS oncogene repression in colon cancer cell lines by G-quadruplex binding indolo[3,2-c]quinolines. *Sci. Rep.-UK*, **5**, 9696.
23. Wen,L.N. and Xie,M.X. (2017) Spectroscopic investigation of the interaction between G-quadruplex of KRAS promoter sequence and three isoquinoline alkaloids. *Spectrochim. Acta A*, **171**, 287–296.
24. Neidle,S. (2016) Quadruplex nucleic acids as novel therapeutic targets. *J. Med. Chem.*, **59**, 5987–6011.
25. Xu,H., Di Antonio,M., McKinney,S., Mathew,V., Ho,B., O'Neil,N.J., Dos Santos,N., Silvester,J., Wei,V., Garcia,J. *et al.* (2017) CX-5461 is a DNA G-quadruplex stabilizer with selective lethality in BRCA1/2 deficient tumours. *Nat. Commun.*, **8**, 14432.
26. Bidzinska,J., Cimino-Reale,G., Zaffaroni,N. and Folini,M. (2013) G-quadruplex structures in the human genome as novel therapeutic targets. *Molecules*, **18**, 12368–12395.
27. Neidle,S. (2017) Quadruplex nucleic acids as targets for anticancer therapeutics. *Nat. Rev. Chem.*, **1**, 0041.
28. Yang,W.Y., Gao,R., Southern,M., Sarkar,P.S. and Disney,M.D. (2016) Design of a bioactive small molecule that targets r(AUUCU) repeats in spinocerebellar ataxia 10. *Nat. Commun.*, **7**, 11647.
29. Luedtke,N.W. (2009) Targeting G-quadruplex DNA with small molecules. *Chimia.*, **63**, 134–139.
30. Felsenstein,K.M., Saunders,L.B., Simmons,J.K., Leon,E., Calabrese,D.R., Zhang,S.L., Michalowski,A., Gareiss,P., Mock,B.A. and Schneekloth,J.S. (2016) Small molecule microarrays enable the identification of a selective, quadruplex-binding inhibitor of MYC expression. *ACS Chem. Biol.*, **11**, 139–148.
31. Howe,J.A., Wang,H., Fischmann,T.O., Balibar,C.J., Xiao,L., Galgoci,A.M., Malinverni,J.C., Mayhood,T., Villafania,A., Nahvi,A. *et al.* (2015) Selective small-molecule inhibition of an RNA structural element. *Nature*, **526**, 672–677.
32. Connelly,C.M., Moon,M.H. and Schneekloth,J.S. (2016) The emerging role of RNA as a therapeutic target for small molecules. *Cell Chem. Biol.*, **23**, 1077–1090.
33. Thomas,J.R. and Hergenrother,P.J. (2008) Targeting RNA with small molecules. *Chem. Rev.*, **108**, 1171–1224.
34. Guan,L.R. and Disney,M.D. (2012) Recent advances in developing small molecules targeting RNA. *ACS Chem. Biol.*, **7**, 73–86.
35. Chen,D.S.H., Yang,H., Kwan,M.H.T., Cheng,Z., Lee,P., Bai,L.P., Jiang,Z.H., Wong,C.Y., Fong,W.F., Leung,C.H. *et al.* (2011) Structure-based optimization of FDA-approved drug methylene blue as a c-MYC G-quadruplex DNA stabilizer. *Biochimie*, **6**, 1055–1064.
36. Castillo-Gonzalez,D., Perez-Machado,G., Guedin,A., Mergny,J.L. and Cabrera-Perez,M.A. (2013) FDA-approved drugs selected using virtual screening sind specifically to G-quadruplex DNA. *Curr. Phram. Des.*, **19**, 2164–2173.
37. Rahman,K.M., Tizkova,K., Reszka,A.P., Neidle,S. and Thurston,D.E. (2012) Identification of novel telomeric G-quadruplex-targeting chemical scaffolds through screening of three NCI libraries. *Bioorg. Med. Chem. Lett.*, **22**, 3006–3010.
38. Gilbert,P. and Moore,L.E. (2005) Cationic antiseptics: diversity of action under a common epithet. *J. Appl. Microbiol.*, **99**, 703–715.
39. Sztuba-Solinska,J., Shenoy,S.R., Gareiss,P., Krumpe,L.R.H., Le Grice,S.F.J., O'Keefe,B.R. and Schneekloth,J.S. (2014) Identification of biologically active, HIV TAR RNA-binding small molecules using small molecule microarrays. *J. Am. Chem. Soc.*, **136**, 8402–8410.
40. Abulwerdi,F.A. and Schneekloth,J.S. (2016) Microarray-based technologies for the discovery of selective, RNA-binding molecules. *Methods*, **103**, 188–195.
41. Griner,L.A.M., Guha,R., Shinn,P., Young,R.M., Keller,J.M., Liu,D., Goldlust,I.S., Yasgar,A., McKnight,C., Boxer,M.B. *et al.* (2014) High-throughput combinatorial screening identifies drugs that cooperate with ibrutinib to kill activated B-cell-like diffuse large B-cell lymphoma cells. *Proc. Natl. Acad. Sci. U.S.A.*, **111**, 2349–2354.
42. Moody,M.R., Morris,M.J., Young,V.M., Moye,L.A. 3rd, Schimpff,S.C. and Wiernik,P.H. (1978) Effect of two cancer chemotherapeutic agents on the antibacterial activity of three antimicrobial agents. *Antimicrob. Agents Chemother.*, **14**, 737–742.
43. Zlotkowski,K., Hewitt,W.M., Sinniah,R.S., Tropea,J.E., Needle,D., Lountos,G.T., Barchi,J.J., Waugh,D.S. and Schneekloth,J.S. (2017) A small-molecule microarray approach for the identification of E2 enzyme inhibitors in ubiquitin-like conjugation pathways. *Slas. Discov.*, **22**, 760–766.
44. Giannetti,A.M., Koch,B.D. and Browner,M.F. (2008) Surface plasmon resonance based assay for the detection and characterization of promiscuous inhibitors. *J. Med. Chem.*, **51**, 574–580.
45. Connelly,C.M., Abulwerdi,F.A. and Schneekloth,J.S. Jr (2017) Discovery of RNA binding small molecules using small molecule microarrays. *Methods Mol. Biol.*, **1518**, 157–175.
46. Carver,J., Dexheimer,T.S., Hsu,D., Weng,M.T., Smith,J.L., Guha,R., Jadhav,A., Simeonov,A. and Luo,J. (2014) A high-throughput assay

for small molecule destabilizers of the KRAS oncoprotein. *PLoS One*, **9**, e103836.
47. Antignani,A., Griner,L.M., Guha,R., Simon,N., Pasetto,M., Keller,J., Huang,M., Angelus,E., Pastan,I., Ferrer,M. *et al.* (2016) Chemical screens identify drugs that enhance or mitigate cellular responses to antibody-toxin fusion proteins. *PLoS One*, **11**, e0161415.
48. Mathad,R.I., Hatzakis,E., Dai,J.X. and Yang,D.Z. (2011) c-MYC promoter G-quadruplex formed at the 5′-end of NHE III1 element: insights into biological relevance and parallel-stranded G-quadruplex stability. *Nucleic Acids Res.*, **39**, 9023–9033.
49. Morgan,R.K., Batra,H., Gaerig,V.C., Hockings,J. and Brooks,T.A. (2016) Identification and characterization of a new G-quadruplex forming region within the kRAS promoter as a transcriptional regulator. *BBA-Gene Regul. Mech.*, **1859**, 235–245.
50. Palumbo,S.L., Memmott,R.M., Uribe,D.J., Krotova-Khan,Y., Hurley,L.H. and Ebbinghaus,S.W. (2008) A novel G-quadruplex-forming GGA repeat region in the c-myb promoter is a critical regulator of promoter activity. *Nucleic Acids Res.*, **36**, 1755–1769.
51. Wei,D.G., Husby,J. and Neidle,S. (2015) Flexibility and structural conservation in a c-KIT G-quadruplex. *Nucleic Acids Res.*, **43**, 629–644.
52. Agrawal,P., Lin,C., Mathad,R.I., Carver,M. and Yang,D.Z. (2014) The major G-quadruplex formed in the human BCL-2 proximal promoter adopts a parallel structure with a 13-nt loop in K+ solution. *J. Am. Chem. Soc.*, **136**, 1750–1753.
53. Yoshida,W., Saito,T., Yokoyama,T., Ferri,S. and Ikebukuro,K. (2013) Aptamer selection based on G4-forming promoter region. *PLoS One*, **8**, e65497.
54. Agrawal,P., Hatzakis,E., Guo,K.X., Carver,M. and Yang,D.Z. (2013) Solution structure of the major G-quadruplex formed in the human VEGF promoter in K+: insights into loop interactions of the parallel G-quadruplexes. *Nucleic Acids Res.*, **41**, 10584–10592.
55. Muller,S., Sanders,D.A., Di Antonio,M., Matsis,S., Riou,J.F., Rodriguez,R. and Balasubramanian,S. (2012) Pyridostatin analogues promote telomere dysfunction and long-term growth inhibition in human cancer cells. *Org. Biomol. Chem.*, **10**, 6537–6546.
56. Wiesner,J., Ortmann,R., Jomaa,H. and Schlitzer,M. (2003) New antimalarial drugs. *Angew. Chem. Int. Edit.*, **42**, 5274–5293.
57. Graber,M., Hell,M., Grost,C., Friberg,A., Sperl,B., Sattler,M. and Berg,T. (2013) Oral disinfectants inhibit protein-protein interactions mediated by the anti-apoptotic protein Bcl-x(L) and induce apoptosis in human oral tumor cells. *Angew. Chem. Int. Edit.*, **52**, 4487–4491.
58. Wang,M.D., Mao,Z.F., Kang,T.S., Wong,C.Y., Mergny,J.L., Leung,C.H. and Ma,D.L. (2016) Conjugating a groove-binding motif to an Ir(III) complex for the enhancement of G-quadruplex probe behavior. *Chem. Sci.*, **7**, 2516–2523.
59. Ma,D.L., Chan,D.S.H., Fu,W.C., He,H.Z., Yang,H., Yan,S.C. and Leung,C.H. (2012) Discovery of a natural product-like c-myc G-quadruplex DNA groove-binder by molecular docking. *PLoS One*, **7**, e43278.
60. Dai,J.X., Carver,M., Hurley,L.H. and Yang,D.Z. (2011) Solution structure of a 2:1 quindoline-c-MYC G-quadruplex: insights into G-quadruplex-interactive small molecule drug design. *J. Am. Chem. Soc.*, **133**, 17673–17680.
61. Ohnmacht,S.A. and Neidle,S. (2014) Small-molecule quadruplex-targeted drug discovery. *Bioorg. Med. Chem. Lett.*, **24**, 2602–2612.
62. Gabelica,V., Baker,E.S., Teulade-Fichou,M.P., De Pauw,E. and Bowers,M.T. (2007) Stabilization and structure of telomeric and c-myc region intramolecular G-quadruplexes: the role of central cations and small planar ligands. *J. Am. Chem. Soc.*, **129**, 895–904.
63. McCormick,F. (2015) KRAS as a therapeutic target. *Clin. Cancer Res.*, **21**, 1797–1801.
64. WHO Expert Committee on the SelectionUse of Essential Medicines (19th: 2013: Geneva Switzerland) and World Health Organization (2014) *The selection and use of essential medicines: report of the WHO Expert Committee, 2013 (including the 18th WHO Model List of Essential Medicines and the 4th WHO Model List of Essential Medicines for Children)*. World Health Organization, Geneva.
65. Zehnder,M. (2006) Root canal irrigants. *J. Endodont.*, **32**, 389–398.
66. Giannelli,M., Chellini,F., Margheri,M., Tonelli,P. and Tani,A. (2008) Effect of chlorhexidine digluconate on different cell types: a molecular and ultrastructural investigation. *Toxicol. In Vitro*, **22**, 308–317.